atmosphere

MDPI

Article

Effects of the Northeast Monsoon on Different Terrain of the Taipei Basin and Lanyang Plain in Taiwan

Pei-Di Jeng and Jou-Ping Hou *

Department of Environmental Information and Engineering, Chung Cheng Institute of Technology, National Defense University, Taoyuan 33551, Taiwan
* Correspondence: hoedwardho@gmail.com

Abstract: The Taipei Basin (TPB) and the Lanyang Plain (LYP) are geographically similar, both situated in northern Taiwan. However, significant differences in heat transfer processes arise between the two regions due to local terrain influences under the Northeast Monsoon. Precipitation patterns in the TPB and LYP, especially during the case study of 26 November 2021, differ markedly due to the distinctive dustpan-shaped terrain of the LYP. Our study, based on the WRF model, reveals that while both the TPB and LYP are characterized by downward cold air transfer, the TPB exhibits stronger atmospheric boundary layer mixing and a higher mixing layer height compared to the LYP. Turbulent kinetic energy (TKE) in the TPB is higher during the morning and evening, while vertical heat flux is more pronounced in the LYP. The average sensible heat flux is greater in the TPB, whereas latent heat flux is higher in the LYP. In addition, the amount of water vapor transported into the LYP by the Northeast Monsoon is greater than in the TPB. In the TPB, the wind field, influenced by the terrain, shifts predominantly from northeast to northeasterly and southeasterly. However, upon entering the LYP, the same environmental wind field is affected by the dustpan-shaped terrain, resulting in a counterclockwise near-surface wind pattern. The wind field transitions from northeasterly in the north to westerly, southwesterly, or northwesterly in the south. This difference in wind field causes precipitation in the TPB to be confined mainly to the windward side of the mountainous areas whereas, in the LYP, precipitation occurs both on the windward side and, more abundantly, in the plains. The effect of different types of terrain under the Northeast Monsoon is quite obvious.

Keywords: northeast monsoon; Taipei basin; Lanyang plain; regional precipitation; terrain effect; heat transfer process

Citation: Jeng, P.-D.; Hou, J.-P. Effects of the Northeast Monsoon on Different Terrain of the Taipei Basin and Lanyang Plain in Taiwan. *Atmosphere* **2024**, *15*, 1527. https://doi.org/10.3390/atmos15121527

Academic Editor: Yubin Li

Received: 16 October 2024
Revised: 12 December 2024
Accepted: 17 December 2024
Published: 20 December 2024

1. Introduction

The East Asian winter monsoon, characterized by cold and dry air masses, primarily originates from the high-latitude inland regions of Siberia and Mongolia. As these cold air masses move southward across East Asia and the adjacent ocean, they absorb heat and moisture, increasing in temperature and humidity [1,2]. Cold air outbreaks, which pass through the ocean and change atmospheric properties, often occur during winter around the world [3–6]. Strengthened northerly winds lead to a significant drop in air temperatures across East Asia [7,8]. Moreover, the prevailing northeasterly winds enhance the cold air's impact on the atmospheric boundary layer from the surface up to 700 hPa [7].

During winter, as the cold air outbreaks meet warmer oceans, they interact with water vapor, forming different types of clouds [9–12]. When the cold air reaches Taiwan, its latent heat flux will be bigger than off the coast from mainland China [13]. This means that the dry and cold properties of the cold air have changed to warm and moist. When the cold air reaches Taiwan, it usually appears in the form of northerly or northeasterly winds, called the Northeast Monsoon in Taiwan [14,15]. The Northeast Monsoon will interact with Taiwan's topography, particularly on windward slopes and coastal areas of northern Taiwan, significantly enhancing orographic precipitation, and resulting in higher

rainfall compared to other regions [16,17]. Precipitation mechanisms differ between coastal windward slopes and plains in northern Taiwan during the Northeast Monsoon. In coastal windward areas, precipitation is primarily driven by orographic lift. As the Northeast Monsoon shifts northerly and wind speeds increase, the combination of oceanic moisture and orographic lift frequently leads to increased rainfall in these regions [18]. When the Northeast Monsoon strengthens, coastal precipitation increases significantly. However, precipitation patterns shift when the monsoon weakens or the wind direction changes [17]. These observations highlight the critical role of the Northeast Monsoon in the precipitation distribution across northern and northeastern Taiwan, with topographic effects and airflow also playing key roles in regional precipitation mechanisms. However, there is no further discussion on the differences in precipitation caused by basin terrain and plain terrain in local areas.

In northern Taiwan, environmental wind fields vary with the intensity and movement of continental cold high-pressure systems. Both the Taipei and Yilan regions are surrounded by mountains. The Taipei Basin (TPB) is relatively flat, whereas the Lanyang Plain (LYP), which is surrounded by mountains on three sides, faces the sea to the east, and has a dustpan-shaped terrain (Figure 1), displays distinct local wind fields under the same Northeast Monsoon conditions. The channel effect on the right side of Datun Mountain is helpful to the advection of water vapor into the TPB and increases the precipitation in the TPB [19]. Numerical simulations indicate that, when stable laminar flow interacts with topography, the behavior of the airflow is influenced by the Froude number. Simulations have shown that, when the Froude number exceeds 1.0, the airflow is capable of crossing over the mountain range, resulting in a minimum wind speed at the peak. Conversely, when the Froude number is below 1.0, part of the airflow is blocked by the terrain and is forced to flow around the mountain. Consequently, the downslope airflow accelerates, forming vortices on the leeward side [20–23]. This interaction between topography and airflow significantly affects the precipitation distribution in local areas of the TPB and LYP [24].

Kabasawa [25], in a report by the Japan Meteorological Agency, observed that, during the Northeast Monsoon, the mid- to low-level airflow was obstructed by the Yilan Mountains, leading to a convergence of westerly and northeasterly winds at lower altitudes. Chen et al. [26] also indicate the impact of orographic lifting and terrain blocking on heavy rainfall in the LYP during the Northeast Monsoon. On the western side of the plain, easterly winds are blocked by the terrain which lifts the moist northeasterly winds, leading to heavy rainfall in the southern mountain regions of the LYP. In other words, atmospheric moisture and topographic effects play equally important roles in the formation and maintenance of heavy rainfall in northeastern Taiwan.

The Yilan Experiment of Severe Rainfall in 2020 (YESR2020) investigated the interaction between complex terrain, winter northeasterly monsoon events, and local circulations in Yilan, Taiwan. The northeasterly monsoon, combined with the humid marine boundary layer, provides a stable low-level moisture flux, which is crucial for heavy rainfall on Yilan's windward slopes and plains. The convergence zone likely results from the interaction between the northeasterly monsoon and orographic precipitation. Terrain-induced local turbulence contributes to heavy rainfall in the southern mountainous areas of Yilan and nearby plains. Thus, the interaction between complex terrain, circulation, and precipitation plays a critical role in rainfall intensity and efficiency [27].

The energy flux transmitted vertically in the atmosphere near the ground is mainly carried out through latent heat flux (LH) and sensible heat flux (SH). The main distribution of the two fluxes is determined by the humidity on the surface. In dry regions, SH dominates whereas, in humid regions, LH becomes more dominant [28]. Heat flux determines the distribution of temperature, humidity, and thickness in the atmospheric boundary layer and atmospheric stability, all of which influence cloud formation and precipitation [29]. Therefore, orographic effects not only influence the wind field and trigger heavy rainfall but also affect vertical energy transport, the vertical structure of atmosphere, and local

circulation within the boundary layer. In the atmospheric boundary layer of the TPB and LYP, due to the different states of the surface, there may be differences in the vertical transport of energy flux. However, no researchers have conducted relevant studies on this in the past.

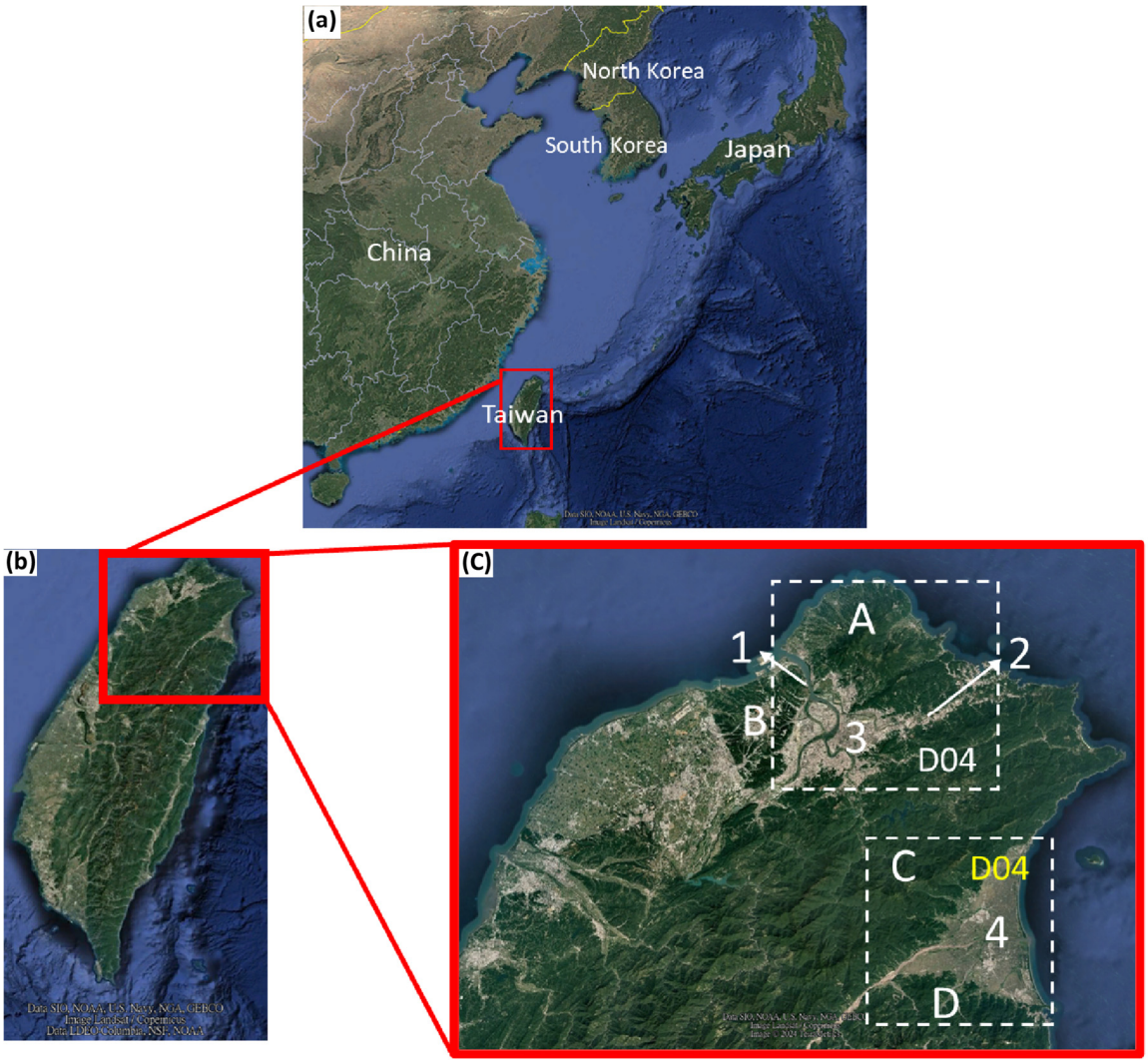

Figure 1. (**a**) Geographical location of Taiwan in East Asia. (**b**) Topography of Taiwan (enlarged view). (**c**) Topography of northern Taiwan (enlarged view). The numbers and English letters in the picture represent, respectively: 1. Tamsui River Basin; 2. Keelung River Basin; 3. Taipei Basin; 4. Lanyang Plain; A: Datun Mountain; B: Linkou Terrace; C: Xueshan Range; D: Central Mountain Range. Map Source: Google Earth. (In (**c**), white and yellow dashed boxes are the innermost domain of four nested domains that our WRF model designed with a horizontal resolution of 0.5 km).

Despite extensive research on the TPB and LYP, relatively few studies have investigated the relationship between environmental wind fields, cold air modification, regional precipitation, and the effects of complex terrain under identical northeasterly monsoon conditions. Taipei and Yilan, located in northern Taiwan and approximately 50 km apart, exhibit significant differences in atmospheric boundary layer characteristics due to their distinct geographic locations and complex terrain. This study uses the Weather Research and Forecasting (WRF) model for numerical simulations, combined with observational data from the Central Weather Administration (CWA) and the Yilan Experiment of Severe Rainfall in 2021 (YESR2021), to analyze how the northeasterly monsoon interacts with these two distinct topographic regions. This research focuses on the influence of large-scale

wind fields, local circulations, and terrain on airflow, and how these factors impact the regional precipitation distribution. In this study, numerical simulations using the WRF (Weather Research and Forecasting) model, combined with observations from the CWA and YESR2021, are used to analyze the impacts of the Northeast Monsoon on these two regions. The focus of this study is to investigate the effects of the large-scale wind field, local circulation, and topographic complexity on the airflow, and to analyze the role of these factors on the regional precipitation distribution. In addition, the similarities and differences in the boundary layer properties of the TPB and LYP under the same large-scale environmental conditions are also analyzed. The remainder of this paper is organized as follows. Section 2 introduces the data and the numerical experiment used in this study. Section 3 provides the simulation results and discussion. The main summary and conclusion are presented in Section 4.

2. Data Analysis and Numerical Experiment

2.1. Synoptic Weather Analysis

Ground-based, satellite, and radiosonde data from the CWA and YESR2021, collected on 26 November 2021, serve as the basis for analysis. The East Asia surface weather analysis (Figure 2a) reveals that a split cold high-pressure system over Inner Mongolia (central pressure 1038 hPa) moved southeastward at 15 km h^{-1}. Taiwan was impacted by the Northeast Monsoon, which is considered to have been modified during its passage over the ocean. The northern coastal areas exhibited thin but abundant cloud cover, with a low-level cloud system throughout the day (Figure 2b).

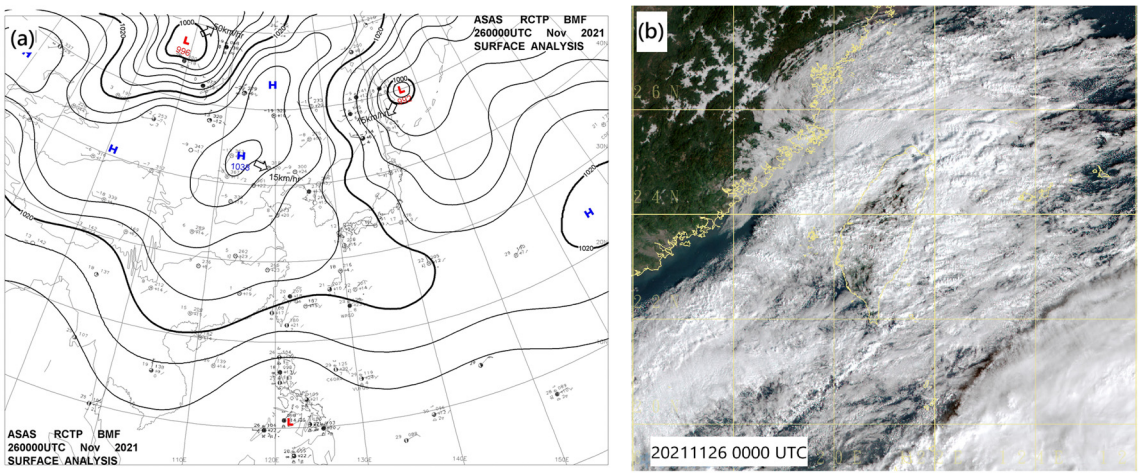

Figure 2. From 0000 UTC on 26 November 2021. (**a**) Surface analysis map of East Asia and (**b**) Himawari-8 true-color satellite imagery of Taiwan.

2.2. Observation Analysis

Surface wind observations at 0100 UTC (0900 LST, UTC+8) and 0400 UTC (1200 LST, UTC+8) in the TPB (Figure 3a,b) indicate that northeasterly winds dominated the northern part of the basin (Figure 3a, light-blue dotted box). Datun Mountain may block portions of the airflow, redirecting it, while other air currents bypass or cross the ridge, resulting in substantial variations in wind direction in the TPB. By 1000 UTC, the winds across most of the TPB had shifted to east–northeast or east–southeast wind (as the red dashed circle in Figure 3b shows) [19–22]. Obviously, the terrain in the northern part of the TPB, in addition to blocking the wind field, will also change the wind field entering the TPB.

At 0100 UTC in the LYP (Figure 4a), the coastal area north of the central LYP exhibited northeasterly to east–northeasterly winds of less than about 2.5 m s^{-1} (or 5 knots) near the surface while, south of the central LYP near the mountainous areas experienced west to northwest winds. The plains to the south of the central region had westerly winds, while the coastal areas observed northwesterly to west–northwesterly winds. The local circulation

of the Northeast Monsoon, influenced by terrain effects, produced counterclockwise circulation and caused wind direction changes (as the slight blue arrow in Figure 4a–c shows). At 0400 UTC (Figure 4b), surface wind speed on the northern side of the LYP slightly increased, with northeasterly to east–northeasterly winds prevailing across the plains, and no westerly winds observed. As the Northeast Monsoon entered the LYP, wind speed decreased to below 2.5 m s^{-1} (or 5 knots), leading to the local counterclockwise flow phenomenon due to the dustpan-shaped topography effect being further away from the mountainous area than at 0100 UTC. By 1000 UTC (Figure 4c), the counterclockwise flow moves to the coastal area. The wind field had shifted to southerly near the mountains. Previous studies by scholars have found that, after the Northeast Monsoon enters the LYP, it will generate a reverse backflow wind field when blocked by the terrain [25–27]. In Figure 4c, a similar situation occurs in the green box near the mountainous area. However, we will further explain the reasons for this phenomenon through subsequent numerical simulations.

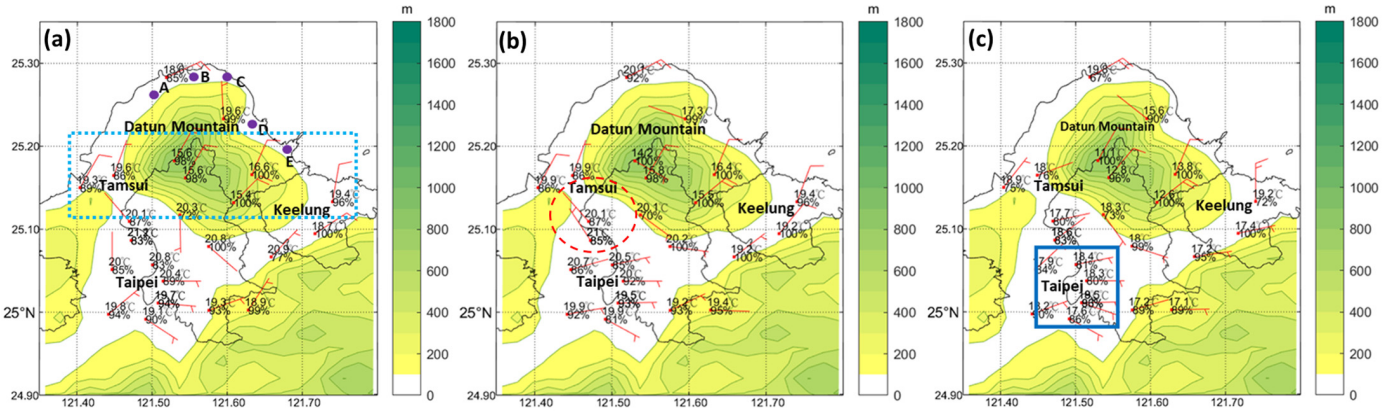

Figure 3. TPB terrain and CWA surface weather station observation data (surface wind field, temperature, and relative humidity) and terrain distribution map on 26 November 2021. The Tamsui, Keelung, and Taipei stations are designated as specific stations. Here, (**a**–**c**) represent 0100 UTC, 0400 UTC, and 1000 UTC, respectively. In (**a**), points A, B, C, D, and E on the northern side of Datun Mountain in the TPB indicate the locations where the Froude number is simulated in Figure 17 using WRF. In (**c**), the blue box represents the selected area for averaging. The light-blue dotted box is the location of the northeast wind in (**a**). The red dashed circle is the location where the Tamsui River enters the TPB in (**b**).

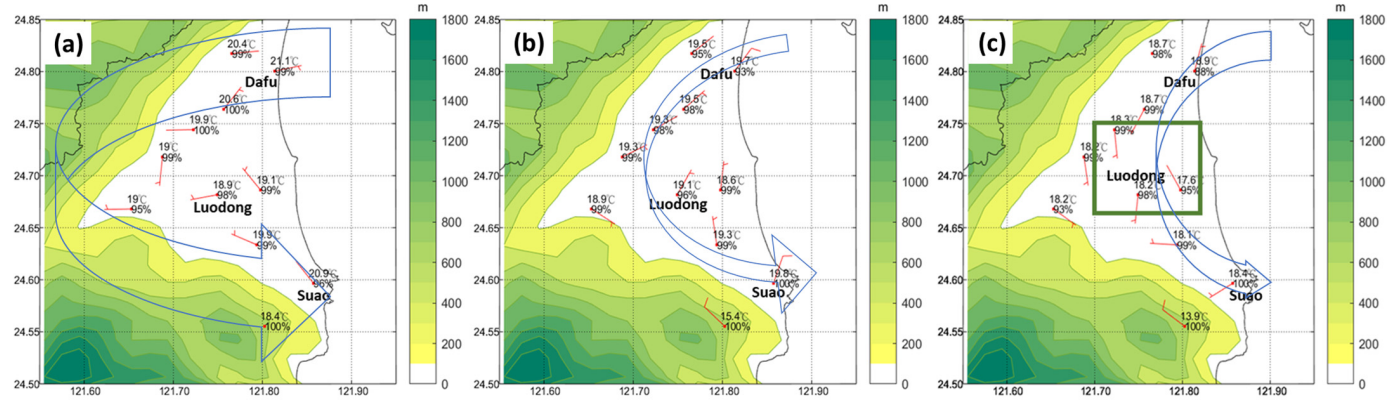

Figure 4. (**a**–**c**) are same times as Figure 3, but for the topography of the LYP in northeastern Taiwan. The Dafu, Luodong, and Suao stations are designated as specific stations. In (**c**), the dark-green box indicates the selected area for averaging. The slight blue arrows represent the local counterclockwise circulation of LYP.

Before 0300 UTC on 26 November, air temperatures near the surface in both the TPB and LYP displayed a pattern of lower temperatures in the north and higher temperatures in the south due to geographic characteristics (as shown in Figure 5, where the stations are arranged from north to south). The cold air associated with the Northeast Monsoon began affecting northern Taiwan on the 26th, particularly after 0300 UTC, when its intensity increased. The first station to be affected was Tamsui in northwestern Taiwan, where the air temperature dropped, followed by Keelung an hour later. Then, at 0500 UTC, air temperatures in Taipei declined. The Dafu and Luodong stations in the LYP showed temperature declines similar to those observed in the TPB, despite Yilan being at a lower latitude. At the Suao station, located near Luodong, the temperature dropped about two hours later than at Dafu and Luodong. By 1100 UTC, air temperatures in the LYP had dropped below those in the TPB. This seems to show that, when the Northeast Monsoon enters northern Taiwan, the air temperature changes are not simply affected by latitude. The LYP, situated at the southern end of the region, showed a faster temperature drop, suggesting that topographic effects and water evaporation may have also contributed to local air temperature variations.

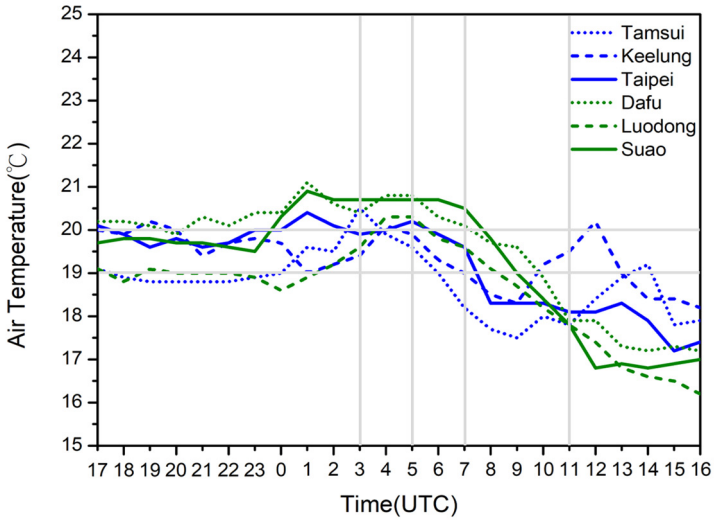

Figure 5. In Figures 3 and 4, the 24 h (from 1700 UTC on the 25th to 1600 UTC on the 26th) time series diagram of the air temperature observed at a specific weather station is shown. The weather stations in TPB are blue lines, the weather stations in LYP are green lines, and the light grayscale lines are specific times and air temperature.

In the Tamsui and Keelung regions, situated outside the TPB, the wind direction was dominantly northerly (Figure 6a). After 1200 UTC, the wind direction began to shift significantly as the cold high pressure from the mainland moved eastward. At the Taipei station of the TPB, the wind direction shifted primarily to easterly, as the topographic effect of the northern TPB blocked northerly winds, forcing the airflow to move around the mountain. At the same time, the wind direction at the three stations located in the north, center, and south of the LYP was influenced by its dustpan-shaped topography, resulting in greater variability.

At the Dafu station in the north, wind direction fluctuated between southerly and northerly before 2100 UTC on the 25th, then shifted to northerly from 2100 UTC on the 25th to 0000 UTC on the 26th, eventually stabilizing as northeasterly. After 1100 UTC, the wind shifted from northwesterly to west–northwesterly. At the Luodong station near the mountains, winds were mostly west–southwesterly before 0400 UTC, with north–northeasterly winds occurring for only about 4 h (i.e., from 0400 UTC to 0800 UTC), before reverting to west–southwesterly after 0000 UTC. This variation indicates that the terrain effects in the LYP may cause the prevailing Northeast Monsoon to induce recirculation, altering local circulation patterns.

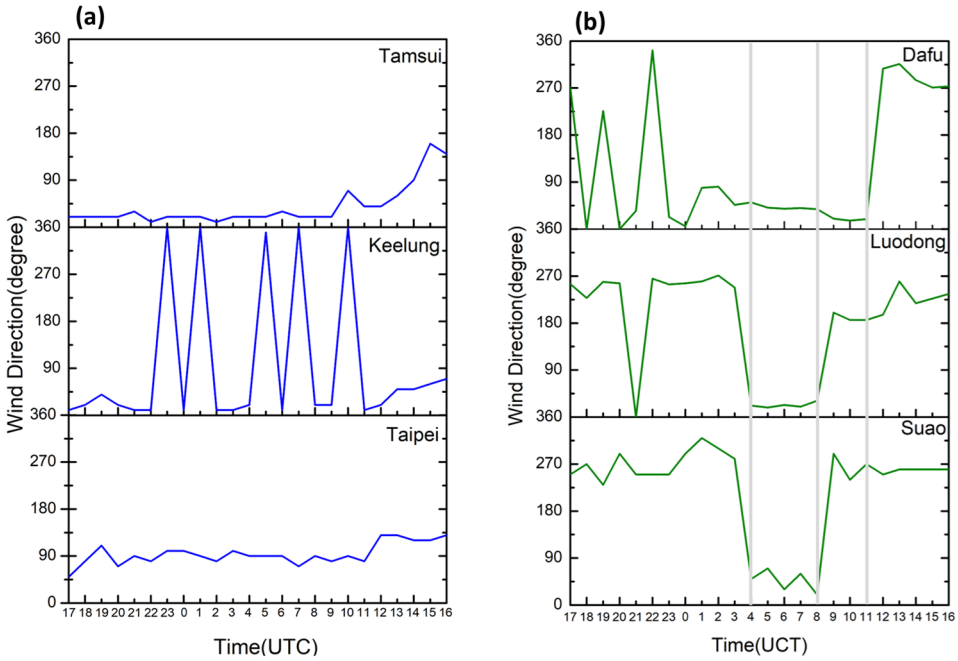

Figure 6. Same as Figure 5, but for the 24 h time series of wind direction (degrees) from 1700 UTC on 25 November 2021 to 1600 UTC on 26 November 2021, for the TPB (**a**) and LYP (**b**). The light gray lines are specific times.

Wind speeds were reduced at the Taipei station due to the topographic barrier effect (Figure 7), while they were higher at the Tamsui and Keelung stations, situated outside the TPB. Wind speed in the LYP was affected by the gradual eastward movement of the cold and high pressure, and varied with wind direction. Wind speeds were more variable at the Dafu and Suao stations on the windward side whereas, at Luodong, closer to the inland mountainous area, wind speed remained relatively stable (Figure 7). The terrain effect has a considerable impact on the wind speed of the TPB and LYP.

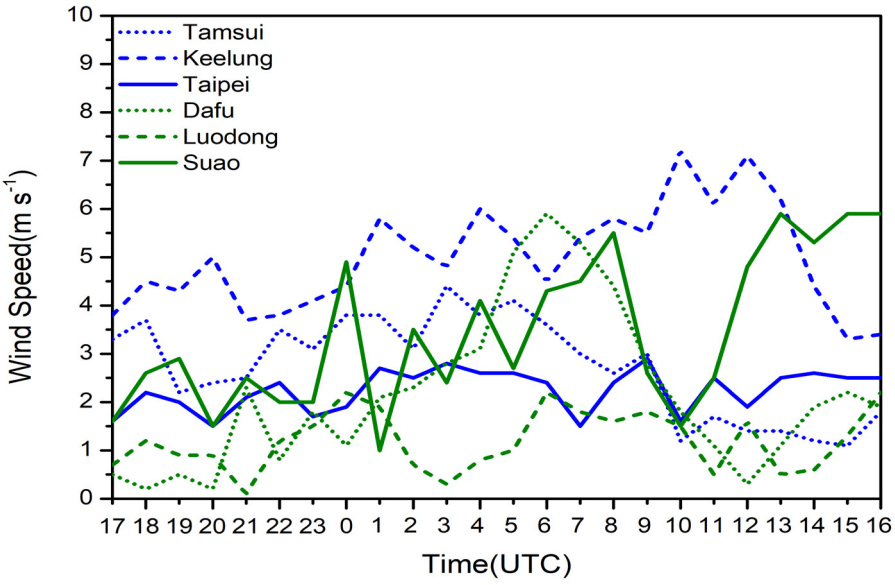

Figure 7. Same as Figure 5, but for the 24 h time series of wind speed (m s^{-1}).

In terms of relative humidity (Figure 8), the LYP exhibited higher levels than the TPB. The Keelung and Dafu stations on the windward side displayed similar relative humidity patterns, while the Tamsui station, located on the northwest side of the TPB, showed

significant fluctuations in relative humidity due to changes in air temperature and wind speed. In contrast, relative humidity at the Taipei station in the TPB and the Luodong station in the LYP exhibited the lowest levels in both regions. Although the observation highlights the influence of the terrain effect, the results of subsequent simulations can further confirm it. These observations suggest that, under the same northeastern monsoon, stations in Taipei and Yilan had significant differences in air temperature, wind field, and relative humidity, attributable to their distinct geographic locations and topographic characteristics. Simulating this characteristic can allow us to better understand the physical reasons for the differences in air temperature, wind field, and relative humidity between the TPB and YPL regions.

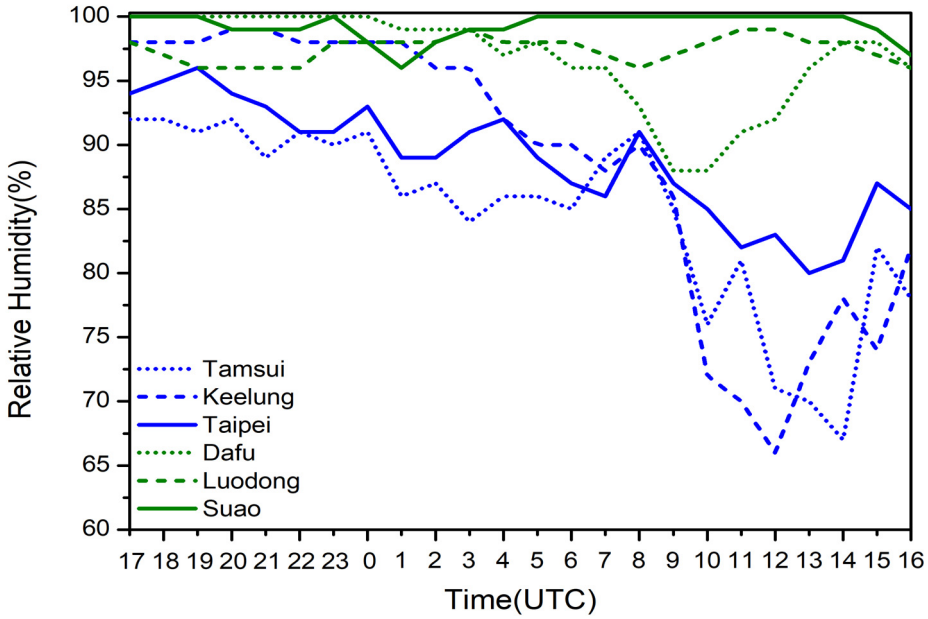

Figure 8. Same as Figure 5, but for the 24 h time series of relative humidity (%).

The accumulated rainfall map (Figure 9) shows that cumulative rainfall in northern Taiwan gradually increased from west to east, with concentrations in northeastern Taiwan and the LYP. The northern region of the TPB was affected by terrain effects, resulting in higher precipitation on the windward side, with some areas accumulating over 110 mm of rainfall. In the eastern and southern regions of the TPB, accumulated rainfall decreased progressively from the estuaries of the Keelung River toward the southwestern basin, with totals below 15 mm. On the leeward side of Datun Mountain and areas east of the Tamsui River, accumulated rainfall was considerably lower, totaling below 10 mm. In contrast, the adjacent LYP displayed distinctly different precipitation patterns and amounts. Rainfall was concentrated in the Suao region on the southern windward side and in the Luodong area of the plains, where totals surpassed 90 mm. Total precipitation in the Yilan mountains was significantly lower than in the plains, a pattern that contrasts with the topographic precipitation effect observed in the TPB. Further study research is required to understand the physical processes underlying these precipitation differences.

To analyze the characteristics of the lower atmosphere in the TPB and LYP under terrain influence, sounding data from the TPB was collected through daily balloon launches by the CWA, while data for the LYP came from the YESR2021 at the Luodong station in Yilan [30]. Sounding data from Taipei (Figure 10a) indicate that the near-surface winds were northeasterly up to about 0.5 km, shifting to southwesterly around 2.5 km, with a lifting condensation level at 0.114 km. Relative humidity in the lower atmosphere, 900 hPa to 850 hPa, was nearly saturated, becoming drier between 850 hPa and 750 hPa. A subsidence inversion was observed above 850 hPa. At Luodong (Figure 10b), near-surface winds were southwesterly or southerly, shifting to northeasterly between 0.9 km and 2 km, before

turning southwesterly above 3 km. The atmosphere near 925 hPa was nearly saturated, with saturation extending down to 725 hPa. Above 725 hPa, the atmosphere became drier, with a subsidence inversion observed at 700 hPa.

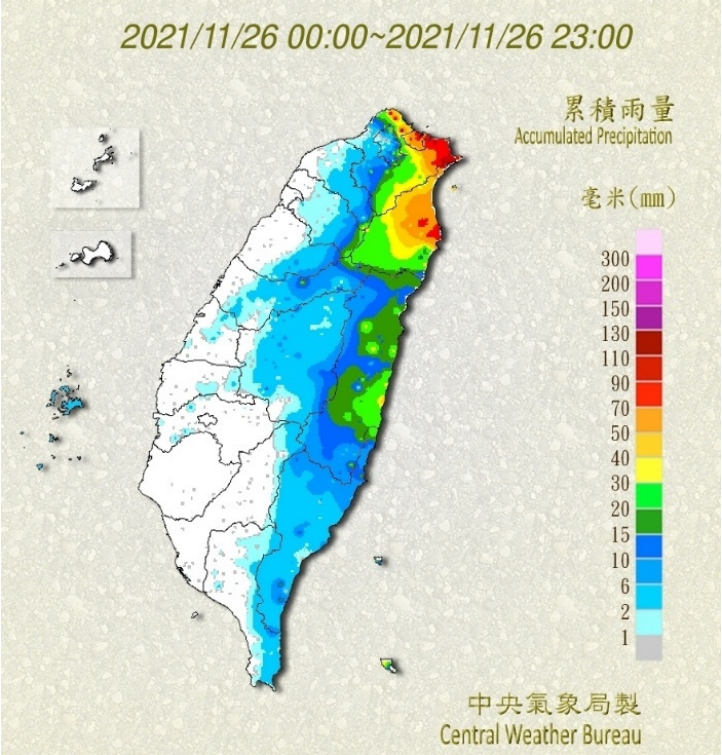

Figure 9. The 24 h accumulated rainfall map of Taiwan on 26 November 2021.

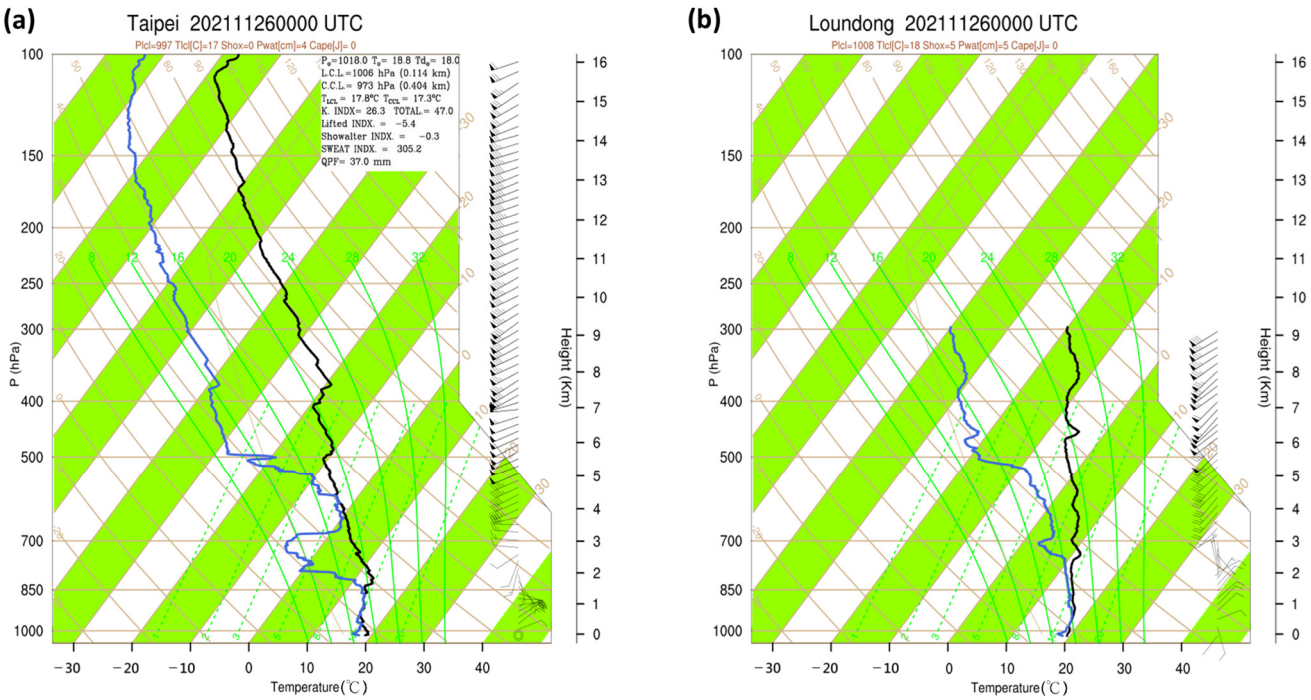

Figure 10. Sounding profiles at 0000 UTC on 26 November 2021, for (**a**) the Taipei station in the TPB and (**b**) the Luodong station in the LYP. The blue curve line represents environmental temperature, and the black curve line represents dew temperature.

The depth of the Northeast Monsoon is below 800 hPa at Luodong and approximately 850 hPa at Taipei. However, due to the location and terrain of the TPB, the depth of Northeast Monsoon at Taipei may be less accurate. In summary, although the locations of Taipei and Yilan are geographically close, significant differences in the thickness of the low-level northeasterly monsoon, cloud development height, and near-surface wind fields are observed, reflecting diverse atmospheric conditions between the two regions. Therefore, it is necessary to use numerical models for physical process analysis.

2.3. Model and Experimental Design

The WRF model is a mesoscale numerical weather prediction system that aims to meet the needs of both atmospheric research and weather forecasting. It has two power cores, a data assimilation system, and a software architecture that is conducive to parallel computing and system scalability. This model provides a wide range of meteorological applications across scales, from tens of meters to thousands of kilometers. Some studies use WRF to simulate terrain effects of valley precipitation enhancement event in winter with a high horizontal space resolution of 0.5 km and get pretty good results [31].

The WRF model allows researchers to generate atmospheric simulations based on actual data (observations and analyses) or idealized conditions. The two power cores of the WRF model are designed according to different purposes, namely, ARW (Advanced Research WRF) and NMM (Non-hydrostatic Mesoscale Model). The two are the same in terms of WRF architecture, but they focus on different aspects. The main physical processes of WRF-ARW can be divided into microphysics, cumulus parameterization, planetary boundary layer, surface processes, and radiation. Jiménez-Esteve et al. [32] studied the impact of land use and horizontal resolution on simulating near-surface atmospheric variables over complex terrain. The results show that, with constant land use data, increasing the horizontal resolution to 0.5 km provides a more detailed representation of terrain features, significantly improving surface air temperature predictions for the valley bottom and slopes.

This study employs the WRF model to simulate the Taipei Basin and Lanyang Plain of Taiwan from 1800 UTC on 25 November to 1800 UTC on 26 November 2021. A four-layer nested grid configuration was used, with the highest spatial resolution of 0.5 km. The initial and boundary conditions were derived from the reanalysis data provided by the National Centers for Environmental Prediction (NCEP), with a horizontal grid resolution of 0.25°. The model comprises 50 vertical layers, 22 of which are below 3 km. The parameterization schemes in WRF were listed as follows: the WRF Single Moment 5 class (WSM5) scheme [33] used for the cloud microphysics process, the MM5 scheme [34] used for the surface layer process, the Yonsei University scheme (YSU) [35] used for the boundary layer process, the Rapid Radiative Transfer Model (RRTM) longwave radiation scheme [36], the Goddard Shortwave scheme [37] for the shortwave radiation, and the Noah land-surface model (LSM) for four soil layers [38]. In addition, cumulus parameterization schemes (CPSs) are not used in this study because convection or deep cumulus clouds typically have a horizontal scale of around 10 km. Thus, models with a 5 km horizontal grid spacing can theoretically resolve these convective processes without additional parameterization [39].

3. Results and Discussion

Through the previous observation and analysis, we found that the TPB and YPL in northern Taiwan show different regional weather characteristics due to different geographical characteristics under the influence of the Northeast Monsoon. In this section, the physical factors causing weather differences are further discussed and analyzed through the simulation results of the WRF model.

3.1. Cold Air Transformation Process

To analyze how cold air is modified across different geographical locations within the TPB and LYP, and to assess the intensity of the Northeast Monsoon relative to terrain,

vertical profile simulations are conducted at three locations in each region (Figure 11). The top of the Northeast Monsoon is estimated at approximately 800 hPa, based on the analysis in Figure 11. Thus, the 10 °C isotherm (as defined by the CWA for cold surges) is used as the reference level for cold air entering northern Taiwan. Comparing the two regions, simulation results indicate that, by 0300 UTC, the 10 °C isotherm at Tamsui, Keelung, and Taipei gradually descended as the vertical temperature gradient steepened, causing cold air to move closer to the surface (Figure 11a–c). The diurnal variation of the 10 °C isotherm in the LYP is similar to that in the TPB. However, the 10 °C isotherm at Dafu is lower than at Luodong and Suao, likely due to the broad, flat terrain of the LYP and Dafu's upstream position relative to the cold airflow. However, the air thickness above 10 °C remains uniform across the region (Figure 11d–f). Vertical temperature fluctuations in the TPB are more pronounced, likely a result of urban heat effects. As the Northeast Monsoon intensified, the volume of cold air moving into both regions increased, causing it to descend from higher altitudes to the surface and bringing the 10 °C isotherm closer to the ground. Simulation results suggest that the terrain in the TPB funneled cold air primarily through the Keelung River valley, leading to variations in cold air thickness across locations. Conversely, the relatively flat terrain of the LYP enables a more uniform cold airflow. As the Northeast Monsoon intensified, cold air descent from the upper layers significantly impacted the vertical temperature gradient. These findings demonstrate that the combined effects of terrain and the Northeast Monsoon led to significant differences in cold air modification between the two regions.

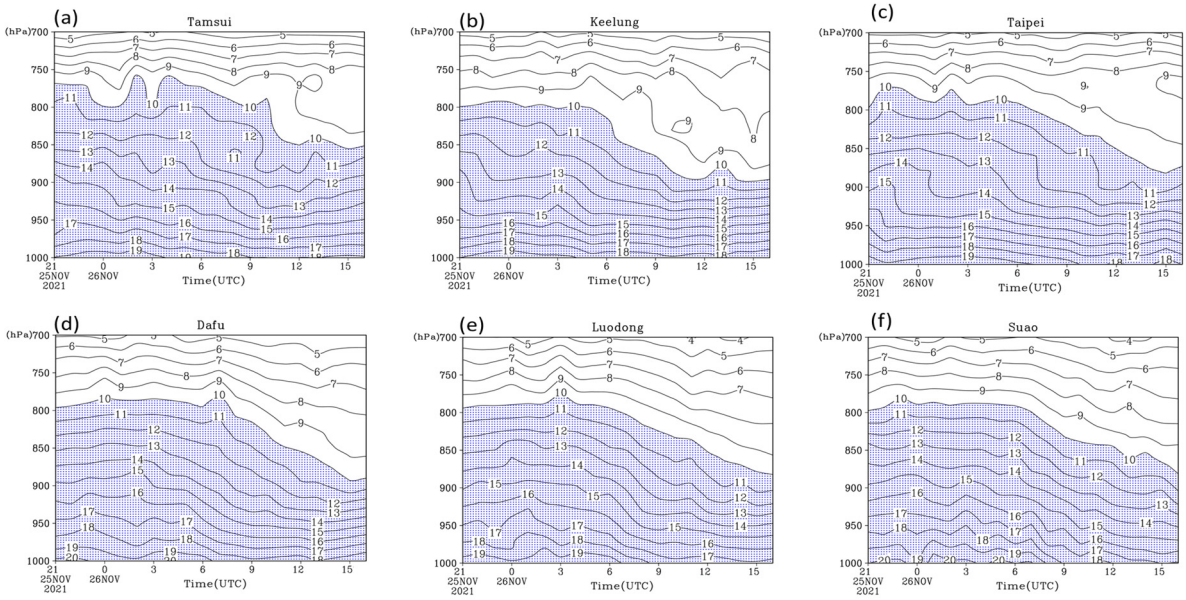

Figure 11. Figure (**a**–**f**) are time series of vertical air temperature profiles at specific stations from Figures 3 and 4, with the blue dotted areas representing the region of air above 10 °C.

Typically, cold air becomes warmer and more humid after passing over the ocean. However, this study found that the cold air moving into northern Taiwan remains relatively cold and dry. As a result, specific humidity gradually decreases at the Tamsui, Keelung, and Taipei stations in the TPB (Figure 12a–c), as well as at the Dafu, Luodong, and Suao stations in the LYP (Figure 12d–f). Notably, specific humidity at Dafu, Luodong, and Suao is higher than in the TPB. This suggests that, as the modified cold air moves into northern Taiwan, moisture content does not increase but decreases. The decrease in water vapor pressure contributes to this trend, while pressure in both the TPB and LYP rises (Figure 12a–f). Additionally, the relatively unobstructed terrain in the LYP facilitated greater moisture advection compared to the TPB, leading to higher specific humidity levels.

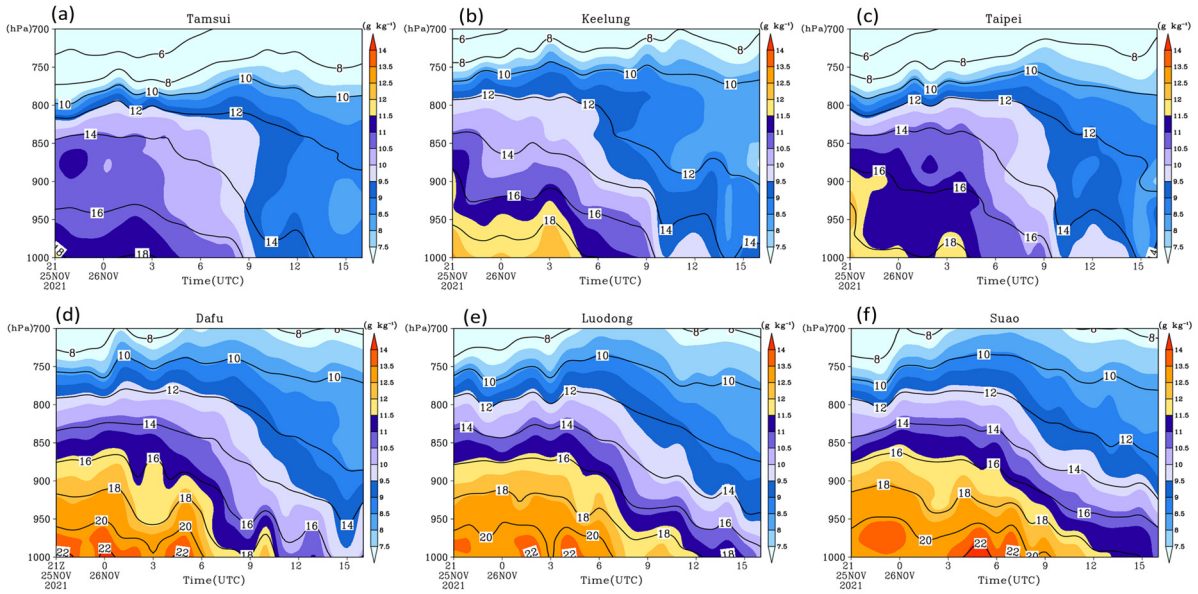

Figure 12. (**a**–**f**) are same spots as Figure 11, but for the vertical of specific humidity. The color shading corresponds to the specific humidity (g kg^{-1}), and the black contour lines are the water vapor pressure (hPa).

3.2. Sensible and Latent Heating Flux

Since the TPB and LYP have different topographic and landform features, in order to understand the difference in energy fluxes of cold air to these two regions, we performed simulations and calculations for SH, LH, and GH. In the TPB, by 2300 UTC on the 25th, the surface heating effect from solar radiation caused SH to gradually increase, peaking at 0200 UTC (Figure 13). A similar pattern was observed in the LYP but, due to its predominantly vegetated surface, SH remains significantly lower than in the TPB. By 0300 UTC in the TPB, SH slightly decreased due to brief scattered rainfall but increased again with radiative heating, peaking at 0400 UTC before gradually declining. Conversely, by 0300 UTC in the LYP, LH had become significantly higher than SH after 0000 UTC, likely due to the increased area of vegetation and recent rainfall. Consequently, LH remains higher than SH for most of the period in the LYP. Furthermore, by 0300 UTC, after LH had reached its peak, rainfall increased atmospheric moisture, but the wind speed gradually decreased, causing LH to decline as well. In terms of ground heat flux (GH), the difference between urban and rural landscapes became more pronounced. Before 0300 UTC, downward GH in the TPB was significantly higher than in the LYP, indicating that the surface heated more rapidly and transferred energy to deeper soil layers. As cold air from the Northeast Monsoon gradually entered the basin, near-surface air temperatures dropped, leading to a decrease in downward GH. Due to the rapid surface cooling, GH reversed, transferring heat back toward the surface.

The topography of both the TPB and LYP plays a crucial role in influencing SH and LH variations. The TPB features basin terrain effects and less precipitation, resulting in consistently higher SH compared to the LYP, both during daytime and nighttime (Figure 13). However, as the Northeast Monsoon intensified, the intrusion of cold air reduced the vertical temperature gradient near the surface, subsequently lowering SH. Additionally, the relatively low rainfall contributes to a reduction in daytime LH. In contrast, extensive vegetation cover in the LYP contributes to lower daytime SH (Figure 13), while the higher rainfall contributes to an increase in LH. The interaction of terrain, rainfall distribution, and cold air intrusion affects heat transfer and dynamic processes within the atmospheric boundary layers in both regions. These factors contribute to variations in the cold air modification processes, resulting in distinct atmospheric properties between urban and rural environments.

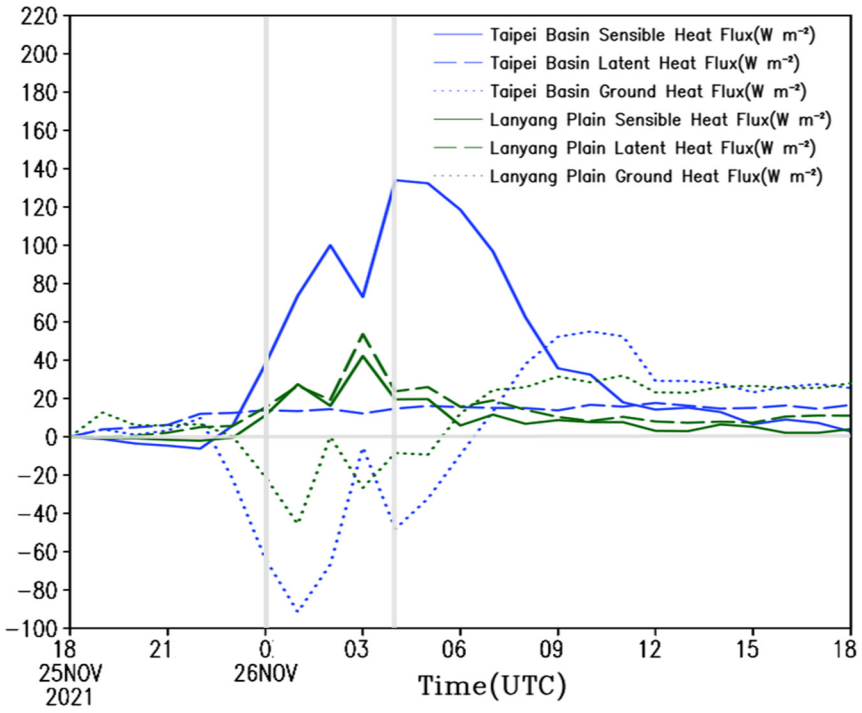

Figure 13. Time series of simulated average sensible heat flux (solid blue and green lines), latent heat flux (dashed blue and green lines), and ground heat flux (dotted blue and green lines) within the blue box in Figure 3c and the green box in Figure 4c. Blue lines represent the TPB, green lines represent the LYP, and light gray lines indicate specific times. The ordinate represents the heat flux density.

3.3. Terrain Effect on Wind Field

Flat areas in the TPB (red box) and LYP (blue box) (Figures 3c and 4c) are selected to spatially average the simulated physical parameters and analyze their variations with altitude to explore how the Northeast Monsoon acts under the influence of different terrains. Simulation results indicate that, as the Northeast Monsoon intensifies, the lower atmosphere wind field in the TPB is influenced by the Keelung River basin, maintaining a relatively stable wind direction from morning to afternoon (averaging east–northeast). In the morning, wind speeds in the lower atmosphere are higher in the TPB compared to the LYP, but this trend reverses in the afternoon. In contrast, the flat terrain of the LYP leads to more pronounced wind shifts, with near-surface winds transitioning from southeast at 0200 UTC to east–northeast by 1000 UTC. In the afternoon, wind speed increases, with the direction shifting once again to east–northeast (Figure 14a,b). Vertical wind shear in the TPB occurs mainly at higher altitudes, contributing to differences in turbulence characteristics between the TPB and LYP, strongly influenced by terrain (Figure 14a).

Through the simulation of wind fields in different directions, it is easier to understand the changes in thickness of the Northeast Monsoon when it passes through different types of terrain. Therefore, we performed wind direction vertical structure simulations for the selected positions of the TPB and LYP in Figures 3c and 4c. Simulation results indicate that the average thickness of the easterly and northerly wind components in the TPB is consistently lower than in the LYP during both morning and afternoon periods, with smaller variations in the thickness of these wind components in the TPB. In the afternoon, as the Northeast Monsoon intensified slightly, the thickness of the northerly wind component in the TPB increased, whereas the easterly wind component became thinner. The reduced variability in wind component thickness within the TPB can likely be attributed to the influence of terrain. In the LYP, where there is no significant terrain blocking the east, morning simulations revealed that the easterly wind was thinner but stronger compared to the afternoon. Overall, the variation in easterly wind thickness in the LYP between morning and afternoon was more significant than in the TPB, with greater variability in

northerly wind thickness and intensity in the afternoon (Figure 15a,b). These findings suggest that, under identical conditions, intensification of the Northeast Monsoon leads to substantial differences in wind field thickness and intensity between these two terrain regions in northern Taiwan. Specifically, wind direction, wind speed, and changes in the wind field exhibit distinct characteristics in both regions. In the LYP, variations in the environmental wind field, influenced by the position of the cold high-pressure system and terrain, are likely key factors influencing the location and intensity of precipitation.

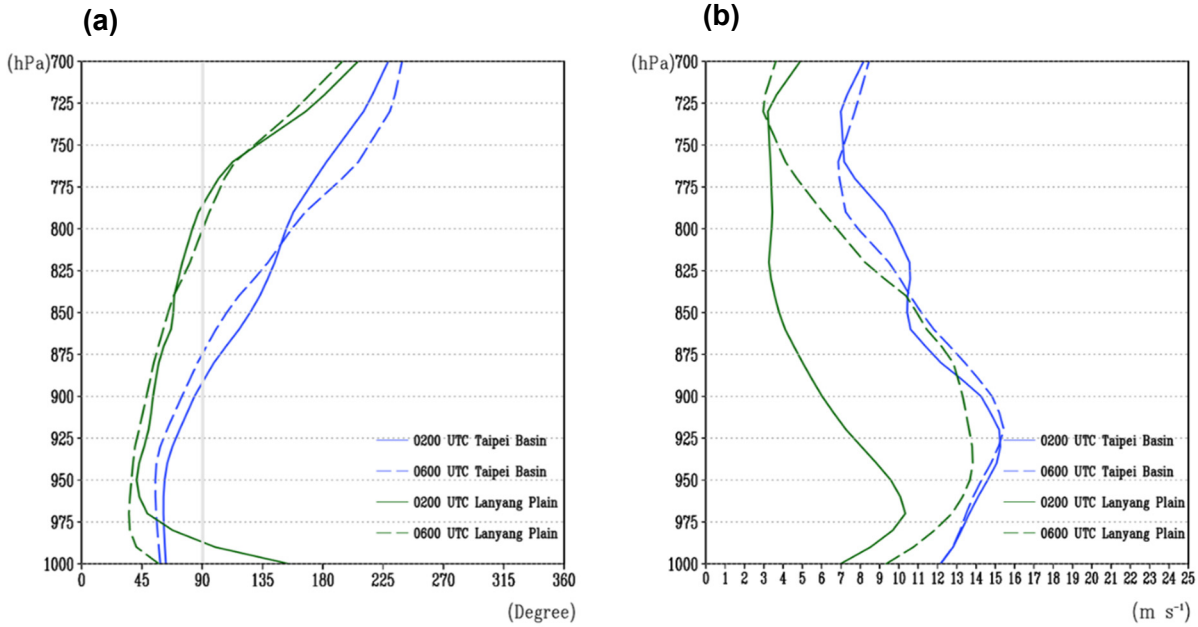

Figure 14. Same as Figure 14, but for (**a**) average vertical profiles of wind direction (degrees) and (**b**) wind speed (m s^{-1}). The light gray line in (**a**) represents easterly wind.

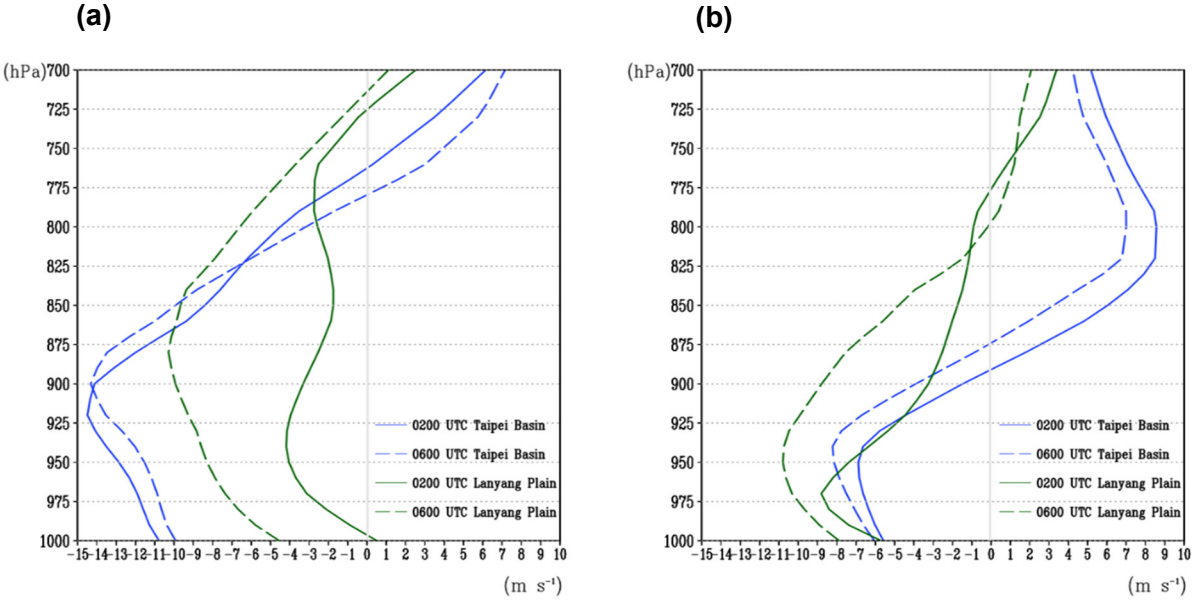

Figure 15. Same as Figure 14, but for the (**a**) zonal wind (U) (m s^{-1}) and (**b**) meridional wind (V) (m s^{-1}). The light gray line represents a calm breeze.

Terrain effects result in higher wind speeds and TKE in the TPB compared to the LYP. As a result, atmospheric mixing below 925 hPa is stronger in the TPB, leading to a higher mixing layer height (Figure 16a,b). Cold air modification processes across different terrains

are significantly influenced by topography, as flux variations reveal distinct dynamic and thermal mechanisms. The complex terrain and valley channeling in the TPB contribute to increased TKE and enhanced vertical atmospheric mixing. As a result, the open topography of the LYP is more conducive to vertical heat flux transfer, particularly during the sinking process of cold air, with more substantial heat exchange occurring in this region. These findings demonstrate that topographic differences distinctly affect flux transfer characteristics, and further illustrate the influence of the cold air modification process on the structure of the atmospheric boundary layer.

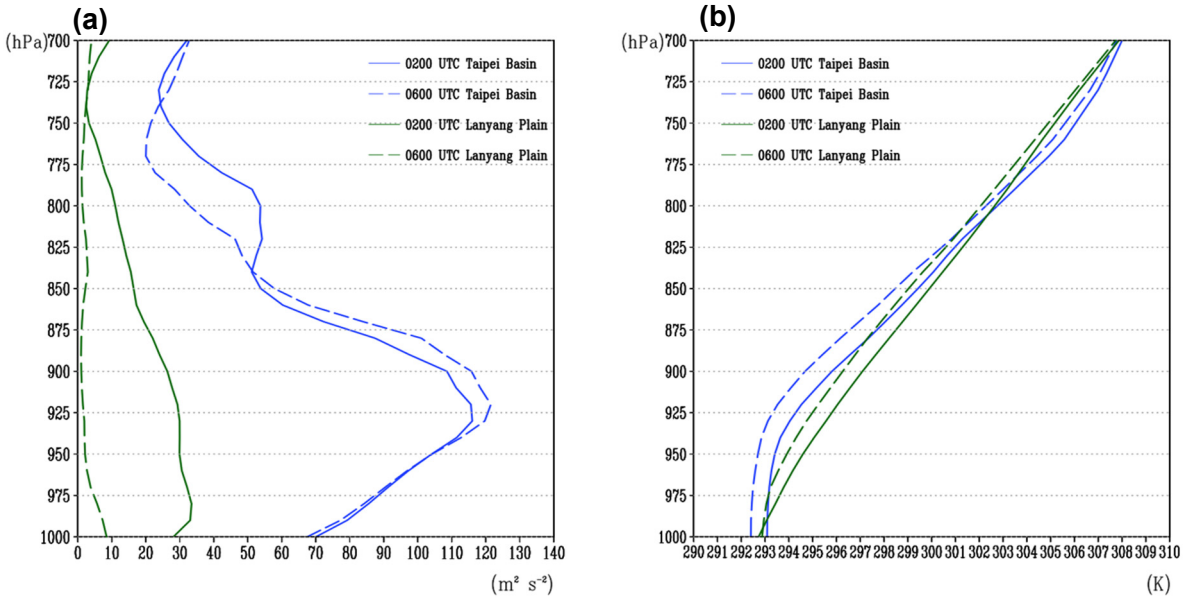

Figure 16. Same as Figure 14, but for (**a**) TKE (m^2 s^{-2}) and (**b**) potential temperature (K). In the figures, the blue lines represent the TPB and the green lines represent the LYP. Solid lines indicate 0200 UTC and dashed lines indicate 0600 UTC.

3.4. TPB and LYP Rainfall Pattern and Amount

Situated on the northern side of the TPB, the terrain of Datun Mountain significantly influences the characteristics of the lower-level Northeast Monsoon airflow. Based on simulation results, we calculated the Froude number (Fr = U/NH, where U is the average upstream wind speed, N is the dry Brunt–Väisälä frequency, and H is the terrain height) [40] for locations A, B, C, D, and E on the windward slope of Datun Mountain to analyze airflow characteristics in the region. The results (Figure 17) show that, from 1800 UTC on 25 November to 1600 UTC on 26 November, the Froude numbers at points B and C exceed 1. When the Froude number exceeds the critical value (close to 1), the Northeast Monsoon can cross the mountain range [41,42]. At point A, the Froude number stays below 1 (green area) in the early morning, while the Froude numbers at points D (yellow area) and E (blue area) remain below 1 throughout the day and part of the night. Idealized model studies suggest that, when the Froude number is less than 1, flow splitting occurs [42]. As the Northeast Monsoon crosses Datun Mountain on the northern side of the TPB, the airflow descends over the mountain and enters the TPB through the Tamsui and Keelung estuaries [32]. Additional simulation results reveal ascending airflow on the windward side of Datun Mountain, accompanied by subsidence on the leeward side (Figure 18a–c). Consequently, no precipitation develops within the TPB. The Northeast Monsoon transports moisture into the basin through the Keelung estuary. This moisture is blocked by the Xueshan Mountain Range to the south, causing it to accumulate in the southeastern part of the basin and gradually decrease toward the northwest. Therefore, precipitation in the TPB is concentrated on the windward side and in the eastern mountainous areas.

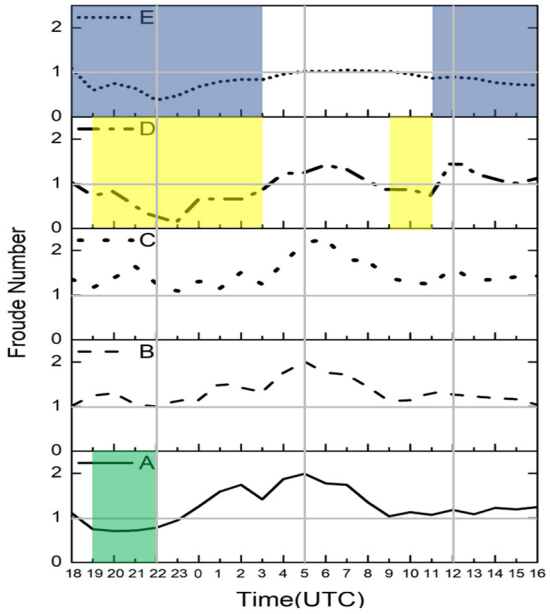

Figure 17. In Figure 3a, Froude number simulation results are obtained at five positions A, B, C, D, and E on the north side of TPB Datun Mountain. The simulation time is from 1800 UTC on 25 November to 1500 UTC on 26 November 2021. The green, yellow, and blue areas are the periods when the Froude number of positions A, D, and E is less than 1, respectively. The vertical light-gray lines represent specific times and the purple line in each figure indicates that the Froude number equals 1.

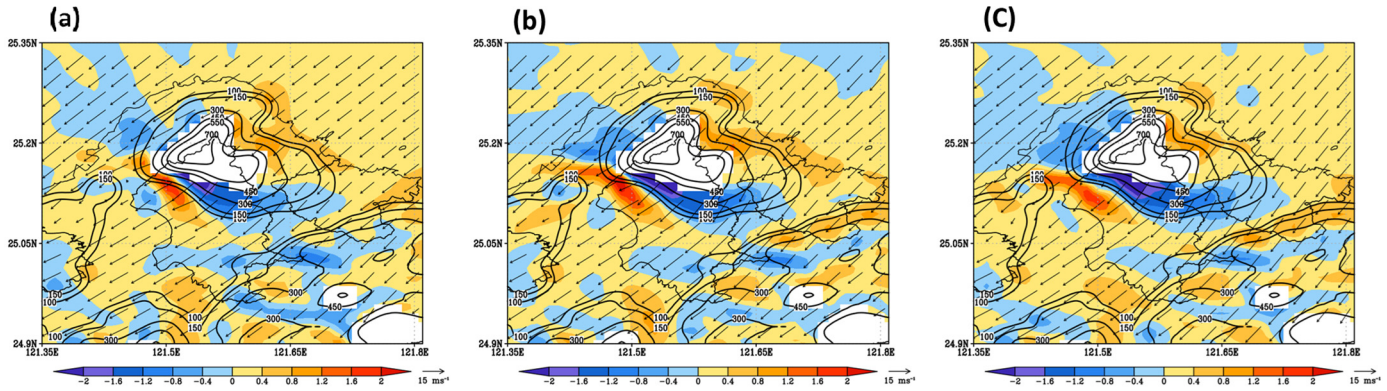

Figure 18. TPB in three different periods at 950 hPa: (**a**) 0100 UTC, (**b**) 0400 UTC, (**c**) 1000 UTC, vertical velocity (m s^{-1}), horizontal wind field (m s^{-1}), and timely accumulated rainfall (mm hr^{-1}) distribution map. The color shading corresponds to vertical velocity and the green dashed lines represent hourly accumulated rainfall at the surface.

Under the same environmental wind conditions, as the Northeast Monsoon moves into the LYP, simulation results show that, at 0100 UTC, north–northeast winds in the LYP generate a counterclockwise recirculation due to terrain effects (Figure 19a). Precipitation is concentrated in the convergence and ascending region formed by the recirculation (Figure 20a), predominantly in the outer part of the plain. Three hours later (Figure 19b), when the wind shifted to northeasterly, the recirculation in the LYP weakened, causing precipitation concentrated in the southern mountainous region. By 1000 UTC, as the wind shifted back to north–northeasterly, the recirculation reappeared in the LYP (Figure 19c), with precipitation once again concentrated in the southern convergence and ascending region (Figure 20c). During this period, the large convergence area in the LYP, combined with moisture advection from the environmental wind field, results in widespread precipitation

across the plain (Figure 20a–c). From the above discussion, it can be seen that the wind direction of the LYP, which is affected by topography, is a key factor leading to the location of precipitation in the LYP. The results of such a wind field simulation are generally the same, although there are some differences from the observations in Figures 3 and 4.

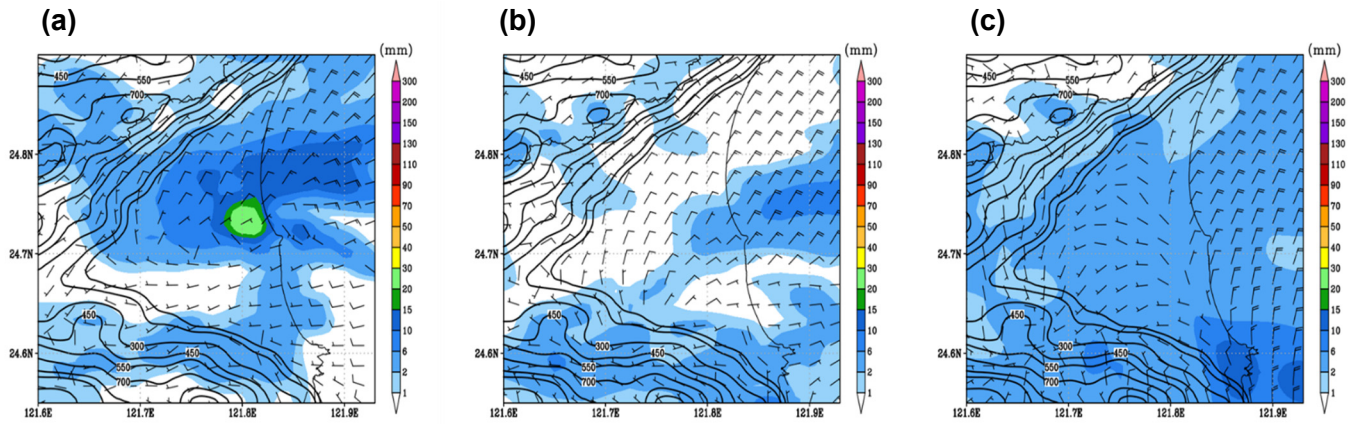

Figure 19. Simulated hourly accumulated rainfall (mm hr^{-1}) in the LYP at different times, (**a**) from 0000 UTC to 0100 UTC, (**b**) from 0300 UTC to 0400 UTC, and (**c**) from 0900 UTC to 1000 UTC. The color shading corresponds to accumulated rainfall.

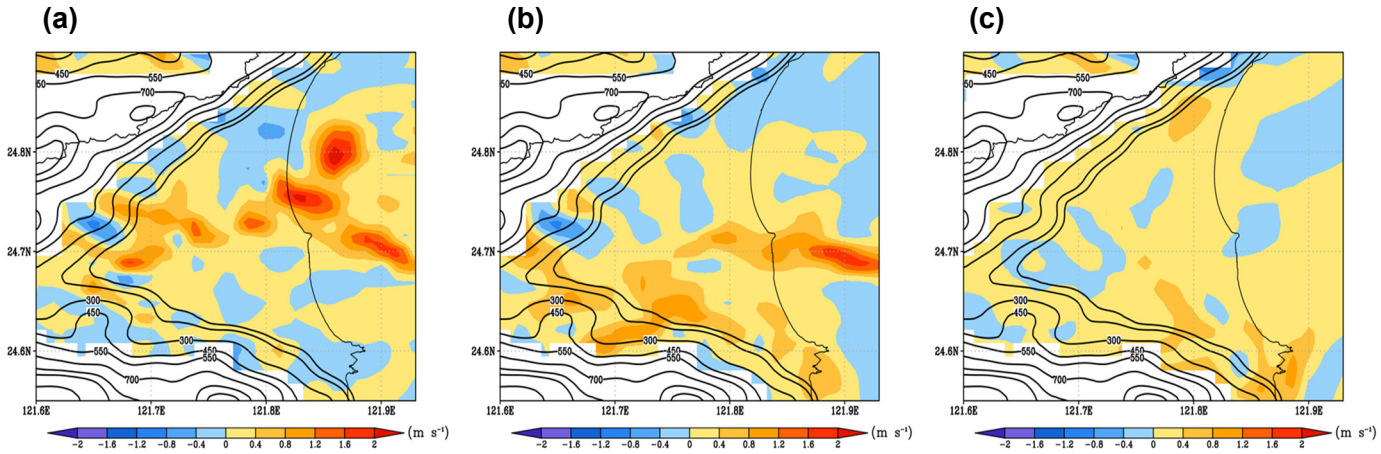

Figure 20. (**a**–**c**) are same times as Figure 18, but for the 950 hPa vertical velocity (m s^{-1}) in the LYP. The color shading corresponds to vertical velocity.

Observations and simulations indicate that the terrain of Datun Mountain significantly influences cold air transport and moisture supply driven by the Northeast Monsoon. Some cold air accumulates on the windward side, while other portions cross the terrain, with the remainder flowing through specific channels, causing noticeable changes in airflow patterns. Conversely, the flat terrain of the Yilan region allows for more uniform airflow and sufficient moisture supply. In the LYP, the dustpan-shaped terrain converges sections of the airflow with the Northeast Monsoon, leading to precipitation not only on the windward side but also across the plains. Thus, precipitation distribution in both regions is closely related to terrain, elevation, airflow patterns, and moisture supply.

4. Summary and Conclusions

In this study, it is found that, although the TPB and the YLP of northern Taiwan are geographically close to each other, they are subject to the same influence of the Northeast Monsoon and differing terrain effects, which result in different changes in the near-surface wind fields, air temperatures, relative humidity, cold air mass transformation processes,

rainfall patterns and distributions, and the characteristics of the low-level atmospheric boundary layer. The results show that, when the Northeast Monsoon enters northern Taiwan, air temperatures are lower at lower latitudes, contrary to expectations of lower temperatures at higher latitudes. As the cold air, having undergone marine transformation, gradually enters North Taiwan, the moisture content in the two areas will decrease rather than increase over time. Furthermore, air temperatures in the LYP, at a lower latitude, decrease more rapidly compared to the higher-latitude TPB. This suggests that local terrain and water evaporation effects significantly influence localized air temperature variations. Relative humidity in the LYP is significantly higher than in the TPB and, similarly, moisture content is higher in the LYP due to terrain effects. Under the same Northeast Monsoon conditions, the differences in air temperatures, relative humidity, and moisture content between the stations in the TPB and LYP can be attributed to their distinct geographic locations and terrain influences.

As the continental cold high pressure shifts eastward, the winds in the TPB and LYP regions change, and the topography on the north side of the TPB blocks the northerly winds and forces the northeasterly monsoon to produce partly over-mountain and partly around-mountain airflow. The Froude number was calculated at five locations on the windward side of Datun Mountain in the northern TPB to analyze the change of airflow characteristics in the area, and found that there are three locations (A, D, and E) where the Froude number is less than 1 for some periods. As a result, airflow enters the TPB around the mountains through the estuaries of the Tamsui and Keelung rivers. At other times, and at locations B and C, the Froude number is greater than 1, allowing the Northeast Monsoon to pass over Datun Mountain in the north of the TPB, so there is a situation in the airflow across the mountain sinks. Further simulation results show that there is a rising area of airflow on the windward side of Datun Mountain, but a subsidence movement on the leeward side. Therefore, there is no precipitation inside the TPB, and the topography of Datun Mountain in the TPB significantly impacts the cold air transport and water supply of the Northeast Monsoon.

It is also found that the dustpan-shaped terrain of the LYP does cause the Northeast Monsoon to produce counterclockwise circulation and partially topographic backflow which, in turn, changes the local circulation pattern in the LYP. The wind field within the LYP is affected by the relative position of cold and high pressure and the topographic effect, which may be the key factors for the location and intensity of precipitation in the region. Therefore, a detailed analysis of the wind field changes and precipitation locations reveals that precipitation is concentrated in the Suao region on the windward side of the southern LYP and in the Luodong area, located on the inner plain. Precipitation in the mountainous areas of the LYP is considerably lower than in the plains, and the local wind field changes influenced by terrain are highly correlated with the precipitation distribution. In the TPB, due to the terrain effect, more precipitation falls on the windward side of Datun Mountain. In the eastern and southern areas of the TPB, the cumulative precipitation decreases from the Keelung River estuary to the southwest of the basin. This precipitation pattern is different from the terrain precipitation effect in the LYP. Therefore, precipitation distribution in both regions is closely related to terrain height, airflow characteristics, and water vapor supply.

There is also a significant difference in the cold air transformation process introduced by the Northeast Monsoon after entering the TPB and the LYP. In terms of TKE, the wind speed in the TPB is higher than that in the LYP due to the terrain effect, and thus the atmospheric mixing condition in the TPB is better below 925 hPa and the height of the mixed layer is higher than that in the LYP. In the low level, energy transfers part of the SH in the TPB, higher than that in the LYP all day due to the complicated topography and urbanization. However, as the Northeast Monsoon intensifies, there is an increase in the amount of incoming cold air, which lowers the vertical temperature gradient near the surface, leading to a decrease in SH and less rainfall, resulting in a lower LH during the daytime. In contrast, the open plain and vegetation cover in the LYP result in lower SH

during the daytime, but more rainfall enhances LH. In the GH component, the downward GH, transferred from the TPB, is much larger than that from the LYP before midday, which means that the surface heats up faster, and more energy can be transferred to the deep soil. With the gradual inflow of cold air into the TPB during the Northeast Monsoon, near-surface air temperature decreases, and the downward transfer of GH also decreases. Because the surface cools down too quickly, the GH starts to transfer heat to the surface in the opposite direction. It can be seen that, after the Northeast Monsoon passes over North Taiwan, the cold air transformation process in both the TPB and LYP has different effects on the flux transfer characteristics through the terrain effect and rainfall distribution, which in turn affects the heat transfer and dynamics in the atmospheric boundary layer of the two regions. It also causes the cold air transformation process to occur over land, resulting in differences in atmospheric properties between the urban and the rural areas. Cold air behind the front would be too thick and the CAPE would vanish, as shown in Figure 2b. Thus, any convection too far to the north could not be supported and developed.

Author Contributions: Conceptualization, J.-P.H.; formal analysis, P.-D.J. and J.-P.H.; funding acquisition, J.-P.H.; investigation, P.-D.J. and J.-P.H.; methodology, P.-D.J. and J.-P.H.; project administration, J.-P.H.; software, P.-D.J. and J.-P.H.; supervision, J.-P.H.; statistical analysis, P.-D.J.; validation, J.-P.H.; visualization, P.-D.J. and J.-P.H.; writing—original draft, P.-D.J. and J.-P.H.; writing—review and editing, P.-D.J. and J.-P.H. All authors have read and agreed to the published version of the manuscript.

Funding: This research was funded by the National Science and Technology Council (NSTC) of Taiwan, under grants NSTC 112-2123-M-002-006, NSTC 113-2123-M-002-018, and NSTC 113-2124-M-002-015.

Data Availability Statement: The WRF model and its user guide are open to researchers and available at https://www2.mmm.ucar.edu/wrf/users/download/get_source.html. Research Data Archive at the National Center for Atmospheric Research, Computational and Information Systems Laboratory, accessed 26 November 2021, https://doi.org/10.5065/D65Q4T4Z.

Acknowledgments: During the preparation of this work, the author(s) used [Google Translate/ChatGPT/Grammarly] to translate, proofread, and check grammar. After using this tool/service, the author(s) reviewed and edited the content as needed and take(s) full responsibility for the content of the publication. Thanks to National Taiwan University for providing weather instruments and AI-related resources.

Conflicts of Interest: The authors declare no conflicts of interest.

References

1. Miao, J.; Jiang, D. Multidecadal variations in the East Asian winter monsoon and their relationship with the Atlantic multidecadal oscillation since 1850. *J. Clim.* **2021**, *34*, 7525–7539. [CrossRef]
2. Zhang, W.; Zhou, T. Impacts of the East Asian Winter Monsoon on Winter Precipitation Variability over East Asia-Western North Pacific. *Clim. Dyn.* **2021**, *57*, 2953–2968. [CrossRef]
3. Rump, B.; Kruspe, G. A Cold Air Outbreak Near Spitsbergen in Spring Time: Boundary Layer Modification and Cloud Development. *Bound.-Layer Meteorol.* **1992**, *61*, 13–46.
4. Chou, S.-H.; Ferguson, M.P. Heat Fluxes and Roll Circulations over the Western Gulf Stream during an Intense Cold-Air Outbreak. *Bound.-Layer Meteorol.* **1991**, *55*, 255–281. [CrossRef]
5. Hein, P.F.; Brown, R.A. Observations of Longitudinal Roll Vortices during Arctic Cold Air Outbreaks over Open Water. *Bound.-Layer Meteorol.* **1988**, *45*, 177–199. [CrossRef]
6. Renfrew, I.A.; Moore, G.W.K. An Extreme Cold-Air Outbreak over the Labrador Sea: Roll Vortices and Air-Sea Interaction. *Mon. Weather Rev.* **1999**, *127*, 2379–2394. [CrossRef]
7. Ding, Y.; Sikka, D.R. Synoptic systems and weather. In *The Asian Monsoon*; Wang, B., Ed.; Springer Praxis Books; Springer: Berlin/Heidelberg, 2006; pp. 131–201.
8. Wang, L.; Lu, M.-M. The East Asian winter monsoon. In *The Global Monsoon System: Research and Forecast*, 3rd ed.; Chang, C.-P., Kuo, H.-C., Lau, N.-C., Johnson, R.H., Wang, B., Wheeler, M.C., Eds.; World Scientific Publishing: Singapore, 2016; pp. 51–61.
9. Atkinson, B.W.; Zhang, J.W. Mesoscale Shallow Convection in the Atmosphere. *Rev. Geophys.* **1996**, *34*, 403–431. [CrossRef]
10. Brümmer, B.; Bakan, S.; Hinzpeter, H. KonTur: Observations of Cloud Streets and Open Cellular Structures. *Dyn. Atmos. Oceans* **1985**, *9*, 281–296. [CrossRef]
11. Kang, S.; Kimura, F. A Numerical Study on the Mechanism of Cloud-Street Formation in the Lee of an Isolated Mountain Near a Coast. *J. Meteorol. Soc. Jpn.* **1997**, *75*, 955–968. [CrossRef]

12. Tsuchiya, K.; Fujita, T. A satellite meteorological study of evaporation and cloud formation over the western Pacific under the influence of the winter monsoon. *J. Meteorol. Soc. Jpn.* **1967**, *45*, 232–250. [CrossRef]
13. Hou, J.-P.; Yu, C.-H.; Chang, C.-S.; Chang, L.-Y.; Tsai, S.-C.; Li, Y.-W.; Huang, C.-H. Numerical study on the modification process of cold air in East Asia. *Atmos. Sci.* **2014**, *42*, 273–300. (In Chinese)
14. Wu, C.; Tsai, I.; Tsai, P.; Tung, Y. Large–scale seasonal control of air quality in Taiwan. *Atmos. Environ.* **2019**, *214*, 116868. [CrossRef]
15. Chan, J.C.L.; Li, C. The East Asia Winter Monsoon. In *East Asian Monsoon*; Chang, C.-P., Ed.; World Scientific Series on Asia-Pacific Weather and Climate; World Scientific: Singapore, 2004; Volume 2, pp. 54–106.
16. Huang, S.-C.; Huang, W.-R.; Wu, Y.-C.; Yu, Y.-C.; Chu, J.-L.; Jou, B.-J.-D. Characteristics and causes of Taiwan's extreme rainfall in January and February 2022. *Weather Clim. Extrem.* **2022**, *38*, 100532. [CrossRef]
17. Chen, C.; Chen, Y. The Rainfall Characteristics of Taiwan. *Mon. Weather Rev.* **2003**, *131*, 1323–1341. [CrossRef]
18. Hung, C.; Kao, P. Weakening of the winter monsoon and abrupt increase of winter rainfalls over northern Taiwan and southern China in the early 1980s. *J. Clim.* **2010**, *23*, 2357–2367. [CrossRef]
19. Lai, L.; Lin, C. Influence of the Geographic Channel Effect on PM2.5 Concentrations over the Taipei Basin about Continental High-Pressure Systems during Winter. *Atmosphere* **2022**, *13*, 1539. [CrossRef]
20. Smolarkiewicz, P.K.; Rotunno, R. Low Froude number flow past three-dimensional obstacles. Part I: Baroclinically generated lee vortices. *J. Atmos. Sci.* **1989**, *46*, 1154–1164. [CrossRef]
21. Sun, W.-Y.; Chern, J.-D.; Wu, C.-C.; Hsu, W.-R. Numerical simulation of mesoscale circulation in Taiwan and surrounding area. *Mon. Weather Rev.* **1991**, *119*, 2558–2573. [CrossRef]
22. Archer, C.L.; Jacobson, M.Z. The Santa Cruz eddy. Part II: Mechanisms of formation. *Mon. Weather Rev.* **2005**, *133*, 2387–2405. [CrossRef]
23. Lin, Y.-L. *Mesoscale Dynamics*; Cambridge University Press: Cambridge, UK, 2007; Volume 630.
24. Chen, C.S.; Huang, J.M. A numerical study of precipitation characteristics over Taiwan Island during the winter season. *Meteorol. Atmos. Phys.* **1999**, *70*, 167–183. [CrossRef]
25. Kabasawa, M. Orographic precipitation of the second kind: A case study. *J. Meteorol. Res.* **1950**, *2*, 1–5. (In Japanese)
26. Chen, C.-S.; Lin, Y.-L.; Zeng, H.-T.; Chen, C.-Y.; Liu, C.-L. Orographic effects on heavy rainfall events over northeastern Taiwan during the northeasterly monsoon season. *Atmos. Res.* **2013**, *122*, 310–335. [CrossRef]
27. Su, H.; Chang, H.; Liu, H.; Chen, T.; Chang, Y.; Chen, P.; Chen, N.; Chung, S.; Hou, P.; Hsieh, K.; et al. Observing severe precipitation near complex topography during the Yilan Experiment of Severe Rainfall in 2020 (YESR2020). *Q. J. R. Meteorol. Soc.* **2022**, *148*, 1663–1682. [CrossRef]
28. Maharana, P.; Kumar, D.; Rai, P.; Tiwari, P.; Dimri, A. Simulation of Northeast Monsoon in a coupled regional model framework. *Atmos. Res.* **2022**, *266*, 105960. [CrossRef]
29. Behrendt, A.; Wulfmeyer, V.; Senff, C.; Muppa, S.K.; Späth, F.; Lange, D.; Kalthoff, N.; Wieser, A. Observation of sensible and latent heat flux profiles with lidar. *Atmos. Meas. Tech.* **2020**, *13*, 3221–3233. [CrossRef]
30. Tsai, T.C.; Hsu, C.H.; Chen, J.R. The development of the "Storm Tracker" and its applications for atmospheric high-resolution upper-air observations. *Atmos. Meas. Tech.* **2020**, *13*, 5395–5412. [CrossRef]
31. Yu, C.; Liu, W.; Cheng, L.; Lin, C. Mechanisms of valley precipitation enhancement over Da-Tun Mountain. *Mon. Weather Rev.* **2022**, *150*, 1851–1871. [CrossRef]
32. Jiménez-Esteve, B.; Udina, M.; Soler, M.; Pepin, N.; Miró, J. Land use and topography influence in a complex terrain area: A high resolution mesoscale modeling study over the Eastern Pyrenees using the WRF model. *Atmos. Res.* **2018**, *202*, 49–62. [CrossRef]
33. Hong, S.-Y.; Dudhia, J.; Chen, S.-H. A revised approach to ice microphysical processes for the bulk parameterization of clouds and precipitation. *Mon. Weather Rev.* **2004**, *132*, 103–120. [CrossRef]
34. Beljaars, A.C. The parametrization of surface fluxes in large-scale models under free convection. *Q. J. R. Meteorol. Soc.* **1995**, *121*, 255–270.
35. Hong, S.-Y.; Noh, Y.; Dudhia, J. A new vertical diffusion package with an explicit treatment of entrainment processes. *Mon. Weather Rev.* **2006**, *134*, 2318–2341. [CrossRef]
36. Mlawer, E.J.; Taubman, S.J.; Brown, P.D.; Iacono, M.J.; Clough, S.A. Radiative transfer for inhomogeneous atmospheres: RRTM, a validated correlated-k model for the longwave. *J. Geophys. Res.* **1997**, *102*, 16663–16682. [CrossRef]
37. Chou, M.-D.; Suarez, M.J. *A Solar Radiation Parameterization for Atmospheric Studies*; NASA Technical Report Series on Global Modeling and Data Assimilation, NASA/TM-1999-104606; NASA Goddard Space Flight Center: Greenbelt, MD, USA, 1999; Volume 15.
38. Ek, M.B.; Mitchell, K.E.; Lin, Y.; Rogers, E.; Grunmann, P.; Koren, V.; Gayno, G.; Tarpley, J.D. Implementation of Noah land surface model advances in the National Centers for Environmental Prediction operational mesoscale Eta model. *J. Geophys. Res. Atmos.* **2003**, *108*, 8851. [CrossRef]
39. Sakradzija, M.; Seifert, A.; Dipankar, A. A stochastic scale-aware parameterization of shallow cumulus convection across the convective gray zone. *J. Adv. Model. Earth Syst.* **2016**, *8*, 786–812. [CrossRef]
40. Baines, P.G. The dynamics of stratified flow over obstacles. *Annu. Rev. Fluid Mech.* **1979**, *11*, 303–327.

41. Smith, R.B. The influence of mountains on the atmosphere. *Adv. Geophys.* **1979**, *21*, 87–230. [CrossRef]
42. Smith, R.B. Hydrostatic airflow over mountains. *Adv. Geophys.* **1989**, *31*, 1–41. [CrossRef]